Structural Analysis of Glazed Tubular Tiles of Oriental Architectures Based on 3D Point Clouds for Cultural Heritage

Ting On Chan[1], Yibo Ling[1], Yuli Wang[1], Kin Sum Li[2], Jing Shen[1]*

[1] School of Geography and Planning, Sun Yat-sen University, 510275 Guangzhou, China - chantingon@mail.sysu.edu.cn, (lingyb3, wangyli56)@mail2.sysu.edu.cn, shenjing@mail.sysu.edu.cn
[2] Department of History, Hong Kong Baptist University, Hong Kong, China - kinsumli@hkbu.edu.hk

Keywords: Glazed tubular tiles, 3D point cloud, Maximum principal curvature, Point cloud segmentation, Structural analysis

Abstract:

Laser scanning, along with its resultant 3D point clouds, constitutes a prevalent method for the documentation of cultural heritage. This paper introduces a novel workflow for the structural analysis of glazed tubular tiles that adorn the roofs of historical buildings in the Orient, utilizing 3D point clouds. The workflow integrates a robust segmentation algorithm utilizing the maximum principal curvature and normal vectors. Moreover, clustering algorithms, including DBSCAN, are incorporated to refine the clusters and thus increase segmentation accuracy. Structural analysis is enabled by cylindrical model fitting, which allows for the estimation of parameters and residuals. While the results exhibit commendable performance in individual tile segmentation, it is imperative to address the impact of substantial variations in scanning range and incident angles before engaging in the structural analysis fitting process. The results of experiment demonstrate that under conditions of significantly large scanning angles, the root mean square error (RMSE) for inadequately fitted tiles can extend to 0.066 m, surpassing twice the RMSE observed for well-fitted tiles. The proposed workflow proves to be applicable and exhibits significant potential to advance practices in cultural heritage documentation.

1. Introduction

The glazed tubular tiles are typically installed with even spacing on the roofs of almost every formal oriental architecture, irrespective of the roof's category (Figure 1). These tiles are specifically designed for rainwater drainage and heat isolation to stabilize the indoor environment (Shen et al., 2022). Additionally, they make a significant contribution to aesthetics.

The use of roof tiles in China can be traced back to the Neolithic period, around the third to second millennium BCE (Peng, 2020; Li and Tang, 2021; Song et al., 2022). The majority of roof tiles dating to this period have been discovered in Northern China, which has led scholars to infer that the use of roof tiles might have stemmed from this region (Peng, 2020; Li and Tang, 2021; Song et al., 2022). Evidence of a more extensive scale of the production of roof tiles can be found within the architectural remains of the capitals of the Qin and Western Han empires from the third century BCE to third century CE, located near the present-day city of Xi’an in Shanxi province (Chen X.W., 2022; Xu, 2023).

(a) (b)

Figure 1. The glazed tubular tiles installed on the roofs of historical buildings: (a) Yuyin Shanfang, Guangzhou, China; (b) Tai Kwun in Hong Kong SAR, China.

A much larger scale of the use of roof tiles in South China can be traced to the remains of the Nanyue state (third to second century BCE) in modern-day Guangzhou, Canton province (Zhang, 2019). The use of roof tiles in the Nanyue state might be one of the possible origins of the use of tubular tiles discussed in this paper. Based on their curvature and shape, roof tiles can range from flat to tubular, each performing distinct functions (Chen, K.Y., 2020). While some tiles may be adored with patterns, others remain undecorated. The addition of decorative patterns implies more input of efforts in manufacture. As integral components of ancient architecture, these tiles serve not only as decorative elements for rooftops but also showcase the exquisite beauty of traditional culture through their distinctive cylindrical form and refined firing techniques.

The tubular tiles can be investigated using the laser scanning techniques. The laser scanning is a commonly-used technique for structural monitoring (e.g., Qi et al., 2014) and finds widespread application in monitoring the structural health of ancient architecture and digital documentation. The output of laser scanning, i.e., the three-dimensional (3D) point clouds, can be processed and analyzed for various specific structures. For instance, Chen et al. (2020) utilized 3D point clouds to estimate small inclination angles of transmission towers for disaster risk reduction. Chan et al. (2021) measured and estimated the degree of symmetry of several Chinese archways based on 3D point clouds obtained from laser scanning. Truong-Hong et al. (2022) developed a new workflow for structural deformation estimation based on 3D point clouds, focusing on the impact of point cloud registration and segmentation on deformation monitoring.

Yang and Xu (2021) introduced intelligent methods for monitoring composite tunnel structures, utilizing visual data to analyse deformation, cracks, and water seepage. The proposed laser-based algorithm enhances reliability, with 3D point clouds verifying water seepage and cracks, while photogrammetry identifies structural issues. Sharma et al. (2022) employed 3D point clouds to assess the structural behaviour of selected columns in the "RGIPT" educational institute in Uttar Pradesh,

* Corresponding author

This contribution has been peer-reviewed. The double-blind peer-review was conducted on the basis of the full paper.
https://doi.org/10.5194/isprs-annals-X-1-2024-19-2024 | © Author(s) 2024. CC BY 4.0 License.

India. They focused on observing and predicting deformation in the columns under vibration loading, demonstrating the effectiveness of lasers in architectural documentation projects such as surveys and renovations. Kaartinen et al. (2022) reviewed the application of 3D point clouds, specifically those obtained from mobile and terrestrial laser scanning, in structural health monitoring. They emphasized detecting cracks, deformation, defects, and changes in various civil infrastructure systems, such as bridges, roads, tunnels, and historical structures. The study highlights the potential of 3D point clouds for efficient and detailed damage detection.

The aforementioned studies on deformation monitoring focused on various structures, attaining high accuracy. However, they rarely investigate the tiles on rooftops for historical buildings. Given the prevalence of glazed tubular tiles in many historical buildings in Asia, especially in China, this paper introduces a novel method specialize in quantifying the structure and the spatial distribution of the tubular tiles. The proposed approach focuses on estimating the maximum principal curvature and normal vector of the 3D point cloud to precisely identify the positions of the tops of these tubular tiles. Subsequently, individual tiles are isolated using clustering techniques, enabling in-depth structural analysis. This methodology allows for the thorough examination of tile structures, contributing to the overall structural health monitoring of the roofs for those historical architecture.

2. Method

The workflow of the proposed method is shown in Figure 2. Initially, the entire roof point cloud data is manually extracted and the principal component analysis (PCA; Nurunnabi et al., 2014) is then applied to align the coordinate axis with the principal component axis. We employ K-D tree for local point cloud construction by searching for neighbouring points, and use PCA to calculate the normal vector for determining the inclination angle. Then, we perform a secondary surface fitting on the local point cloud to compute its maximum principal curvature.

Initial thresholds are set for the inclination angle and curvature to roughly extract the point cloud representing the top arc of the tubular tile, with these thresholds determined through a trial-and-error approach. Principal component analysis is then applied on the rough top arc point cloud and the coordinates are transformed to a system with the three principal component directions as the basis. The roof point clouds are projected along the Z-axis (Figure 3) and the Z-values is used to compute the grayscale for each grid. A clustering algorithm is adapted to adaptively determine segmentation thresholds for binarization, creating a mask. This mask is then applied to the rough top arc point cloud of the tubular tile to obtain the accurately extracted top arc point cloud.

Following this, we project the accurate top arc point cloud of the tubular tile along the X/Y-axis. We then use a clustering technique to segment each top arc point cloud of the tubular tile and count the segments. Finally, the original tubular tile point cloud is used with the segmented top arc of the tubular tile as a reference. We group the points for each tubular tile based on Euclidean Distance to perform segmentation for the subsequent structural analysis.

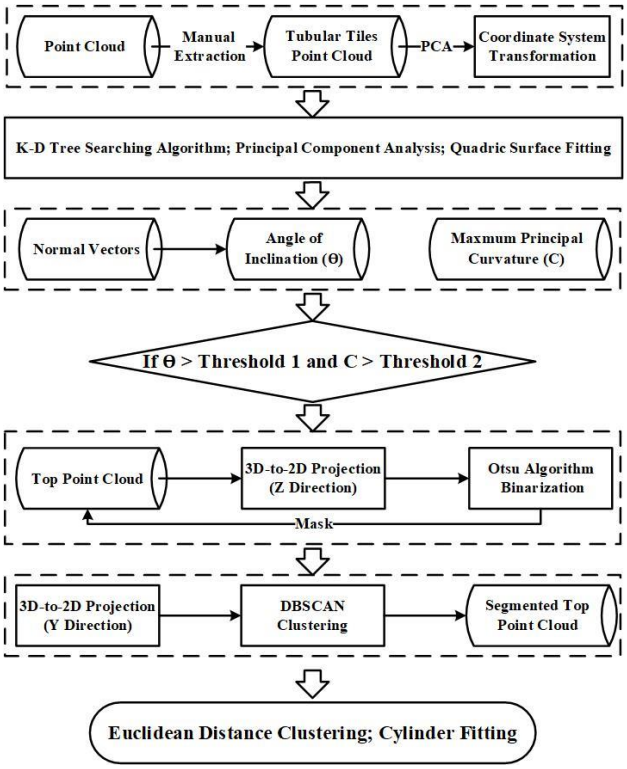

Figure 2. Workflow of the proposed method.

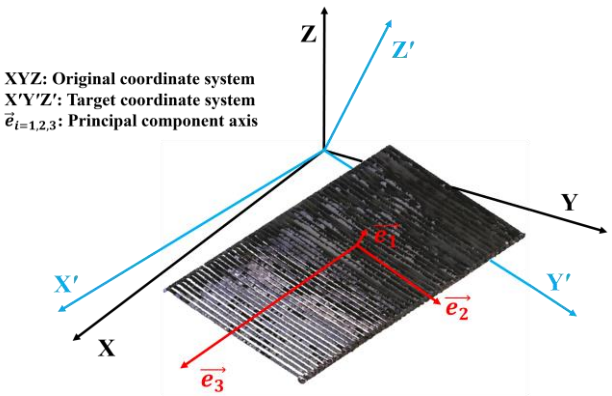

Figure 3. Coordinate systems: red stands for coordinate system created by the PCA; blue stands for the coordinate system of the scanner space.

2.1 Maximum Principal Curvature and Normal Vector

We utilize the planar model (Chan et al., 2015) in which the points are aligned to a nearby surface characterized by k-nearest points. After establishing the planar coefficients, it becomes possible to ascertain the first and second derivatives concerning the x and y parameters at each surface point. This allows for the estimation of Gaussian and mean curvature (Gray, 1997) for every individual point (Figure 4) within the point cloud:

$$K = \frac{f_{xy}^2 - f_{xx} \cdot f_{yy}}{\left(1 + f_x^2 + f_y^2\right)^2} = k_1 k_2 \quad (1)$$

$$H = \frac{\left(1+f_x^2\right) f_{yy} - 2 f_x f_y f_{xy} + \left(1+f_y^2\right) f_{xx}}{2\left(1+f_x^2+f_y^2\right)^{\frac{3}{2}}} = \frac{1}{2}\left(k_1 + k_2\right) \quad (2)$$

where K = Gaussian curvature
H = mean curvature
k_1, k_2 = principal curvature

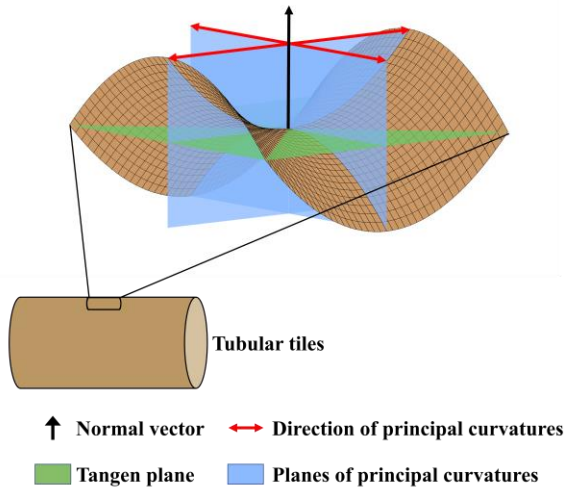

Figure 4. Maximum principal curvature of the tubular tiles.

Meanwhile, normal vectors for each point in the point cloud, are computed to analyze the geometrical properties of tiles. We use the PCA to estimate local normal vectors using the k-nearest neighbor (KNN) algorithm, searching for the nearest k points around each point (Sanchez et al., 2015), as illustrated in Figure 5.

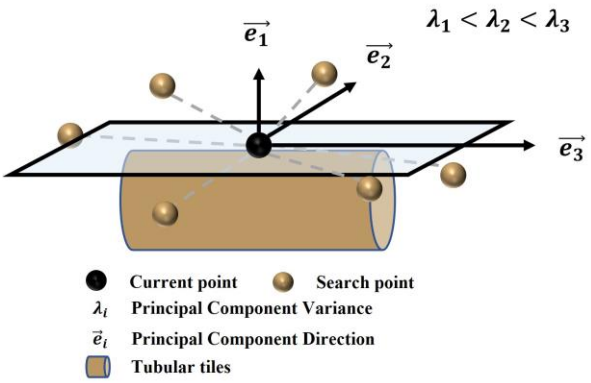

Figure 5. *K*-mean neighbour for principal curvature and normal vector estimation.

2.2 3D-to-2D Projection

After passing the maximum principal curvature and orientation threshold, the points are projected along the Z-direction, generating a raster image with Z values as grid values. Subsequently, the Otsu algorithm (Otsu, 1979) is employed to determine the threshold for binarization, resulting in a mask image. When applied to the point cloud, this process can group points with lower heights. The projection is illustration in Figure 6.

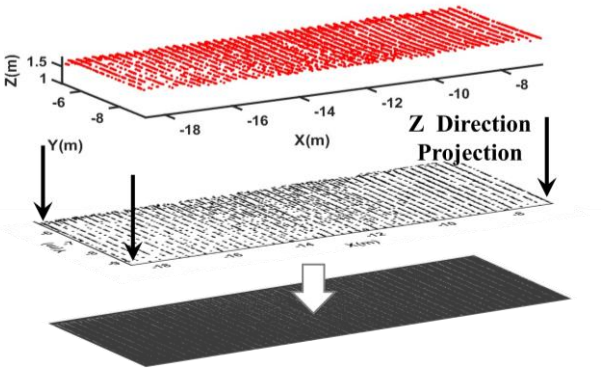

Figure 6. 3D-to-2D (Z-direction) projection.

2.3 Tubular Tile Segmentation

We employ the Density-Based Spatial Clustering of Applications (DBSCAN, Ester et al., 1995) to segment individual tubular tiles after obtaining the point cloud at the highest or near-highest position of each tubular tile from the above procedures with a Y-direction projection, as shown in Figure 7. DBSCAN does not require specifying the number of clusters beforehand and can discover clusters of arbitrary shapes, based on two main parameters: (1) ε, the radius within which the algorithm looks for neighboring data points, and (2) minPts, the minimum number of data points required to form a cluster. These thresholds are initially set by visually estimating the spacing between categories, and then continuously adjusting them through a trial-and-error approach.

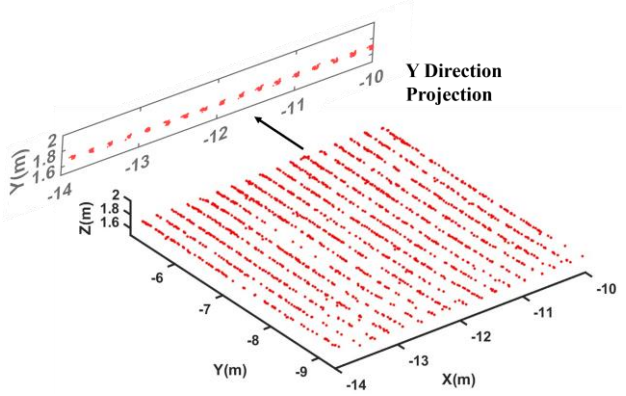

Figure 7. Y-direction projection.

2.4 Structural Analysis

The tubular tiles are mostly cylindrical structure. To monitor its deformation, we perform RANSAC cylinder fitting (Moritani et al., 2019) for each individually segmented tubular tiles obtained via the proposed workflow. Based on the estimated model parameters and residuals, we can compare different tubular and access their deformation from a perfect cylinder. Figure 8 demonstrated the best-fit cylinder for a point cloud of the tubular tile. The cylindrical model (Chan et al., 2015) is:

$$f(x_c, y_c, \Phi, \Omega, r) = X'^2 + Y'^2 - r^2 \quad (3)$$

$$\begin{pmatrix} X' \\ Y' \\ Z' \end{pmatrix} = \mathbf{R}_2(\Phi)\mathbf{R}_1(\Omega)\begin{pmatrix} X - x_c \\ Y - y_c \\ Z \end{pmatrix} \quad (4)$$

where (x_c, y_c) is the centre of the best-fit cylinder on the x-y plane, Ω and Φ are the rotation angles for the rotation matrices $\mathbf{R}_1$ and $\mathbf{R}_2$, which correspond to rotations about the x-axis and y-axis, respectively; and r is the radius of the best-fit cylinder.

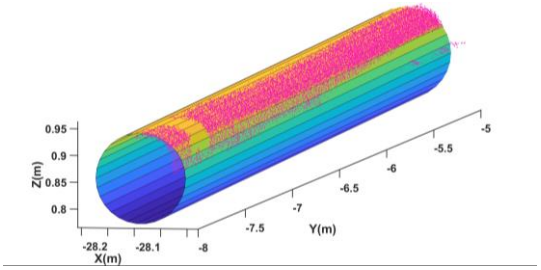

Figure 8. Best-fit cylinder of the tubular tile point cloud (magenta).

3. Experiments

The 3D point clouds of Guan’s ancestral hall in Panyu, Guangzhou, China, were collected using a Trimble SX 10 in July, 2022. Our focus is on the roofs (Roofs 1, 2 and 3) shown in Figure 9. We manually extracted the point clouds of the roofs (e.g., Roof 2 is shown in Figure 10) as the input for our proposed approach. Roofs 1, 2, 3 consist of 95492, 901149, and 735001 points, respectively.

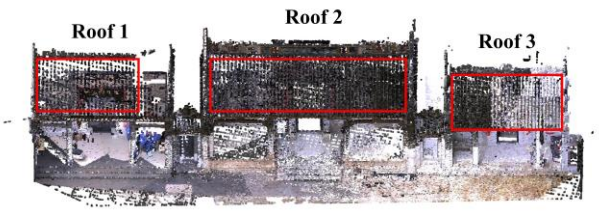

Figure 9. Point cloud of Guan’s ancestral hall (Panyu, Guangzhou, China).

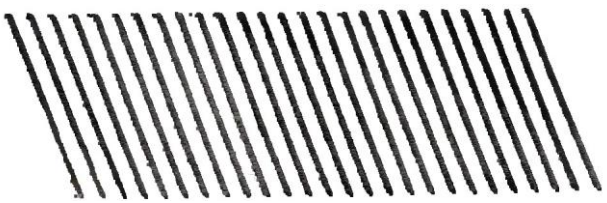

(a)

(b)

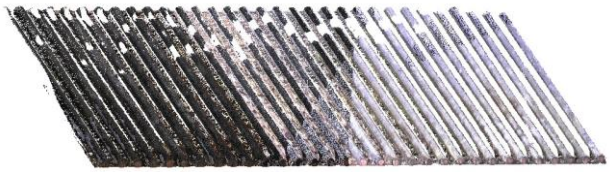

(c)

Figure 10. Point cloud of tubular tiles by manual extraction: (a) Roof 1; (b) Roof 2; (c) Roof 3.

4. Results

4.1 Tubular Tile Segmentation

Figure 11 shows the roof points of Roof 2 (with the largest area) after the 3D-to-2D projection and binarization were applied. Specially, in the figure, it can be seen that the banalization outcomes before and after the highest points are kept. It can also be seen that the tops of each individual tubular tile are almost all perfectly preserved due to the banalization. This achieves the intermediate-segmentation for the subsequent refinement process. The original points (before the highest points are kept) contain many points at lower position connecting each tubular tiles to hinder the segmentation.

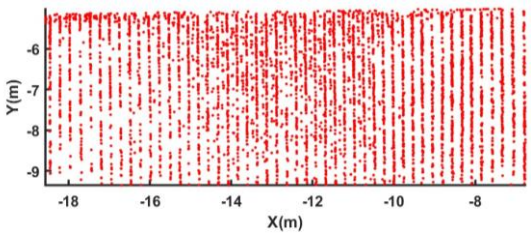

(a)

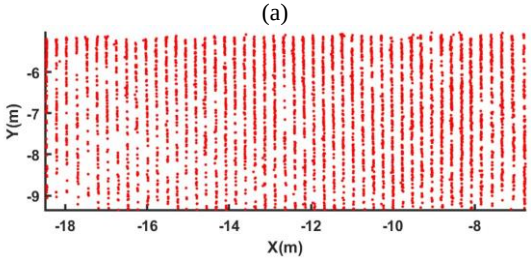

(b)

Figure 11. Roof points of Roof 2 after the 3D-to-2D projection and binarization: (a) before the highest points are kept; (b) after the highest points are kept.

After the DBSCAN was applied, the segmented points of the top of each individual tubular tiles for Roofs 1, 2, and 3 are shown with distinct colours in the Figure 12. It can be seen that even some of the points are missing, the segmentation outcomes are still promising. This is attributed to the fact that the Y direction projection can weaken the impact of the missing points along the Y-axis as all points are projected into the X-Z planes. The point density is not unified due to the different incident angles of the laser beams, especially when the roof was scanned by a static scanner mounted on a tripod.

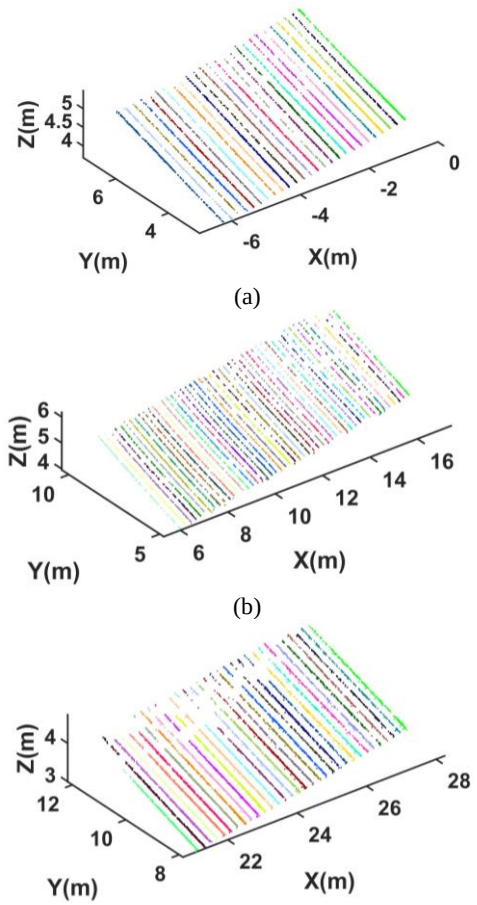

(a) (b) (c)

Figure 12. Segmented points of the top of each individual tubular tiles after the DBSCAN is applied: (a) Roof 1; (b) Roof 2; (c) Roof 3.

As the segmented points at the top after applying the DBSCAN do not always contain the entired structure for each tubular tile, individual windows are created with an Euclidean Distance threshold (e.g., an approxiately radius of each tubular tiles) to perform a quick point aggregation to obain the full point cloud (Figure 13) of each individual tubular tile. The accuracy of the segementation for Roofs 1-3 match exactly with the counts from the point clouds based on visual inspection. After indivdiual tubular tile is segmented, the stuctural analysis can be performed with the full point cloud.

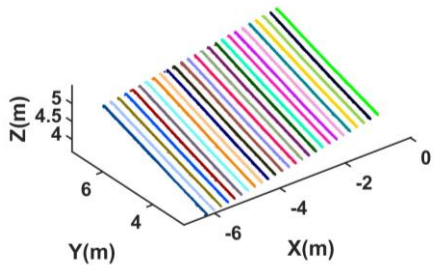

(a)

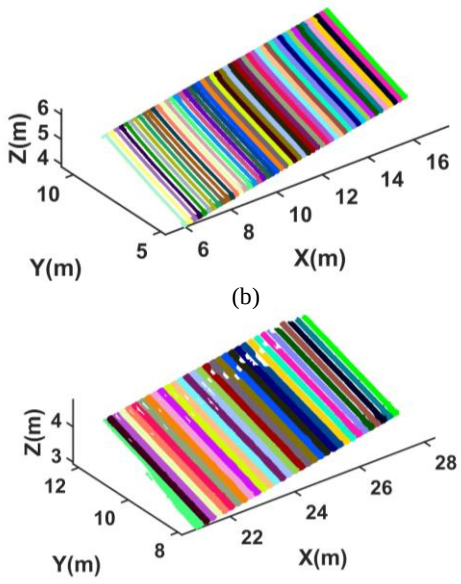

(b)

(c)

Figure 13. Full point clouds of each tubular tiles after point aggregation based on Euclid Distance: (a) Roof 1; (b) Roof 2; (c) Roof 3.

4.2 Structural Analysis of the Tubular Tiles

Figure 14a shows the best-fit cylinders overlapping the point cloud of the tabular tiles on the left side of Roof 3. The point cloud is relatively sparser compared to the right side due to the longer scanning range and larger incident angles. As seen in Figure 14b, the best-fit cylinder is much more uniform. Therefore, we conclude that ensuring the high quality of the point clouds plays a crucial role in subsequent structural analysis. The effect of high variation in scanning range and incident angles can be compensated for before the structural analysis fitting is performed. Nevertheless, for the left side of Roof 3 shown in Figure 14b, we observe a slight variation in the fitting, such as the estimated radii of the best-fit cylinder for the tiles. This slight variation is likely due to the actual fluctuation in the shape of the neighbouring tubular tiles. Upon visual inspection, we can see that the tiles are not perfectly uniform, possibly due to limited manufacturing and installation standards.

A residual analysis (Chan et al., 2016) was conducted on the fitting results for Roof 3, and the outcome was tabulated in Table 1. Since the segmentation method solely employs the Euclidean distance as a single threshold, the results shows the inclusion of some point clouds at the junctions between cylindrical tiles. Additionally, the estimated radius of the cylindrical tiles is at the centimetre level. Upon comparing the fitting results of incomplete and relatively complete point clouds, the latter exhibits an average root-mean-square-error (RMSE) higher than the former by 0.038 m, with a discrepancy in estimated radii of 0.037 m, while the ground truth is defined as 0.05 m based on manual measurement from the point cloud. The results show that around one third of the tile on Roof 3 has similar geometry and severity of deformation, when the effect of high variation in scanning range and incident angles have not yet been compensated.

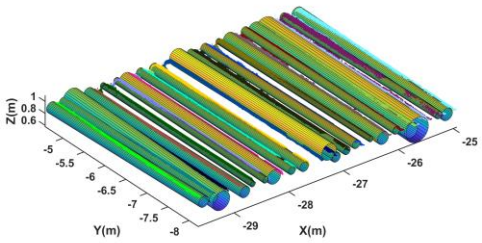

(a)

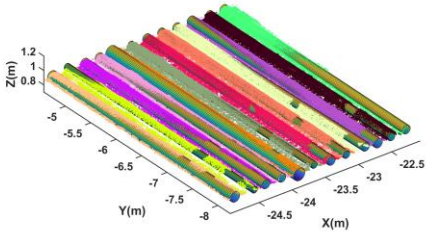

(b)

Figure 14. Best-fit cylinder for the tubular tiles on Roof 3: (a) left side; (b) right side.

Table 1. RMSE and estimated radius of the best-fit cylinder for the tubular tiles on Roof 3.

	Tubular tiles point cloud	
	bad	good
No. of cylinder	20	12
Average RMSE of residuals (m)	0.066	0.028
Average estimated radius (m)	0.102	0.065

5. Conclusion

In this paper, we present a workflow focusing on the structural analysis of glazed tubular tiles that cover the roofs of most historical buildings in the Orient, based on 3D point clouds. The workflow incorporates a robust segmentation algorithm that utilizes the maximum principal curvature and normal vectors. Additionally, clustering algorithms, such as DBSCAN, are embedded in the workflow to enhance accuracy. We applied this workflow to three sets of point clouds from separate roofs of a historical building in China. The individual tubular tiles are accurately segmented for subsequent structural analysis. The results indicate that compensating for the high variation in scanning range and incident angles is crucial to achieving a thorough analysis of every tile installed on the roof. Specifically, the error in poorly-fitted tiles can reach 0.066 m, which is more than twice the error for well-fitted tiles, as the tiles were scanned with large incident angles. Overall, the workflow proves applicable and demonstrates great potential for facilitating cultural heritage documentation.

References

Chan, T.O., Lichti, D.D., Belton, D., 2015. A Rigorous Cylinder-based Self-Calibration Approach for Terrestrial Laser Scanners. *ISPRS Journal of Photogrammetry and Remote Sensing*, 99, p. 84-99.

Chan, T.O., Lichti, D., Belton, D., Klingseisen, B., Helmholz, P., 2016. Survey accuracy analysis of a hand-held mobile LiDAR device for cultural heritage documentation. *Photogrammetrie - Fernerkundung - Geoinformation*, 10 (3), 153-165.

Chan, T.O., Sun, Y., Yu J., Zeng, J. and Liu, L., 2021. Symmetry etection and Analysis of Chinese Paifang Using 3D Point Clouds. *Symmetry*, 13, 2011.

Chen K.Y., 2022. A Comprehensive Review of the Study on Tubular Tile Unearthed in China. *Changzhou Wenbo Collection*, 2022(00), 50-57. [In Chinese].

Chen, M., Chan, T.O., Wang, X., Lin, Y. Luo, M., Huang, H., Sun, Y., Cui, G., Huang, Y., 2020. A Risk Analysis Framework for Transmission Towers under Potential Pluvial Flood - LiDAR Survey and Geometric Modelling. *International Journal of Disaster Risk Reduction*, 50, 101862.

Chen X.W., 2022. Study of Tile Eaves from the Han Dynasty Chang'an City. *Journal of Archaeology*, 2022(01), 1-18+149-150. [In Chinese].

Ester, M., Kriegel, H.P., Xu, X., 1995. *A database interface for clustering in large spatial databases*. 2. Inst. für Informatik.

Gray, A., 1997. The gaussian and mean curvatures. *Modern differential geometry of curves and surfaces with mathematica*, 2, 373-380.

Kaartinen, E., Dunphy, K., Sadhu, A., 2022. LiDAR-Based Structural Health Monitoring: Applications in Civil Infrastructure Systems. *Sensors*, 22(12), 4610.

Li, Y.L., Tang, Y.W., 2021. Research on the Origin and Early Development of Architectural Pottery Tiles. *Frontier Archaeology Research*, 2021(2), 157-172. [In Chinese].

Moritani, R., Kanai, S., Date, H., Watanabe, M., Nakano, T., Yamauchi, Y., 2019. Cylinder-based efficient and robust registration and model fitting of laser-scanned point clouds for as-built modeling of piping systems. *Comput. Aided Des. Appl*, 16, 396-412.

Nurunnabi, A., Belton, D., West, G., 2014. Diagnostics based principal component analysis for robust plane fitting in laser data. *16th Int'l Conf. Computer and Information Technology*. *IEEE*, 484-489.

Otsu, N., 1979. A threshold selection method from gray-level histograms. *IEEE transactions on systems, man, and cybernetics*, 9(1), 62-66.

Peng, X.J., 2020. The relationship between prehistoric terracotta and cave dwelling architecture. Cultural relics in the spring and autumn, 2020(6), 3-10. [In Chinese].

Qi, X., Lichti, D.D., El-Badry, M., Chan, T.O., El-Halawany, S.I., Lahamy, H., Steward, J., 2014. Structural Dynamic Deflection Measurement with Range Cameras. *Photogrammetric Record*, 29 (145), 89-107.

Sanchez, J., Denis, F., Coeurjolly, D., Dupont, F., Trassoudaine, L., Checchin, P., 2020. Robust normal vector estimation in 3D point clouds through iterative principal component analysis.

ISPRS Journal of Photogrammetry and Remote Sensing, 163, 18-35.

Sharma, V.B., Dubey, R., Bhatt, A., Bharadwaj, S., Srivastava, A., Biswas, S., 2022. a Method for Extracting Deformation Features from Terrestrial Laser Scanner 3d Point Clouds Data in Rgipt Building. *The International Archives of the Photogrammetry, Remote Sensing and Spatial Information Sciences*, 43, 267-272.

Shen, J., Li, L., Wang, J.P., Li, X., Zhang, D., Ji, J., Luan, J.Y., 2021. Architectural glazed tiles used in ancient chinese screen walls (15th–18th century AD): Ceramic technology, decay process and conservation. *Materials*, 14(23), 7146.

Song, J.N., Chang, J.Y., Ma, Z.M., 2022. Study on pottery pottery of Longshan period in Loess Plateau area. Archaeology and Cultural Relics, 2022(2), 119-131. [In Chinese].

Truong-Hon, L., Lindenbergh, R., Nguyen, T. A., 2021. Structural asessment using terrestrial laser scanning point clouds. *International Journal of Building Pathology and Adaptation*, 40(3), 345-379.

Xu, L.G., 2023. A study on brick and pottery in Chang 'an City of Han Dynasty. *Journal of Archaeology*, 2023(4), 459-482. [In Chinese].

Yang, H., Xu, X., 2021. Structure monitoring and deformation analysis of tunnel structure. *Composite Structures*, 276, 114565.

Zhang, J., 2019. Bricks and tiles unearthed from the Nanyue State Palace Administration site and their production. *Journal of Cultural Heritage*, 2019(3), 66-74, 93. [In Chinese].